TD-DFT STUDY OF TOLUIDINE BLUE O IN AQUEOUS SOLUTION: VIBRONIC TRANSITIONS AND ELECTRONIC PROPERTIES

Kostjukov V.V., Leontieva S.V., Savchenko E.V., Rybakova K.A., Voronin D.P.
Sevastopol State University
Universitetskaya st., 33, Sevastopol, 299053, Russia; e-mail: Viktor_Kostukov@mail.ru
Received 22.07.2022. DOI: 10.20930/rusjbpc.2022.0534

Abstract. The vibronic absorption spectrum of Toluidine blue O (TBO) dye in an aqueous solution was calculated using the time-dependent density functional theory (TD-DFT). The calculations were performed using all hybrid functionals supported by Gaussian16 software and 6-31++G(d,p) basis set with IEFPCM and SMD solvent models. The IEFPCM gave underestimated values of λ_{max} in comparison with the experiment, what is a manifestation of the TD-DFT "cyanine failure". However, the SMD made it possible to obtain good agreement between calculated and experimental spectra. The best fit was achieved using the X3LYP functional. The dipole moments and atomic charges of the ground and excited states of the TBO molecule were calculated. Photoexcitation leads to an increase in the dipole moment of the dye molecule. An insignificant photoinduced electron transfer was found in the central ring of the chromophore of the TBO molecule. Vibronic transitions play a significant role in the absorption spectrum of the dye.
Key words: *Toluidine blue O, aqueous solution, vibronic absorption spectrum, time-dependent density functional theory, electronic properties*

INTRODUCTION

Toluidine blue O (3-amino-7-(dimethylamino)-2-methylphenothiazin-5-ium, TBO, Fig. 1) is a thiazine dye discovered by William Henry Perkin in 1856.

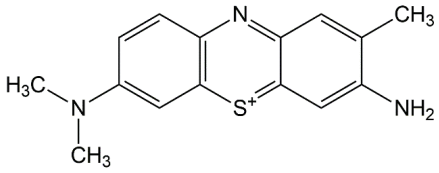

Figure 1. The Toluidine blue O molecule

TBO is widely used in photodynamic therapy of bacterial infections [1-8], for staining tissues and cells [9-11], as well as in biosensors (together with nanostructures) [12-16], solar cells [17] and semiconductor nanocomposites [18]. The therapy of Alzheimer's disease with TBO based on its inhibition of Tau protein aggregation is promising [19]. Using optical methods, it was found that the TBO molecule is able to effectively bind to DNA [20-26], RNA [26-28], proteins [19,29-34], silver nanoparticles [6,35,36], silica [15] and cadmium sulfide [37], natural organic matter [38], cyclodextrins [39-41], surfactant micelles [40-42], chitosan [43], heparin [44], nanotubes [2], fatty acids [45] , polysaccharides [9,46-48] and other polymers [18,49,50]. Numerous experimental optical studies of TBO itself have been carried out - aggregation [21,51-54], reduction [36,42,55-57], photodegradation [58-60], metachromasia [61-63], polymerization [16,64] and photophysical properties of TBO in solutions [51,52,54,65,66], thin films [67–70], in the solid amorphous phase [53], and on a gold electrode [64]. However, theoretical studies of the optical properties of TBO have not yet been carried out. In particular, the absorption spectrum of the dye was not calculated.

METHODS

In an excited state, not only the electronic energy of the molecule changes, but also the vibrational energy, i.e. the molecule undergoes an electronic-vibrational (vibronic) transition (Fig. 2).

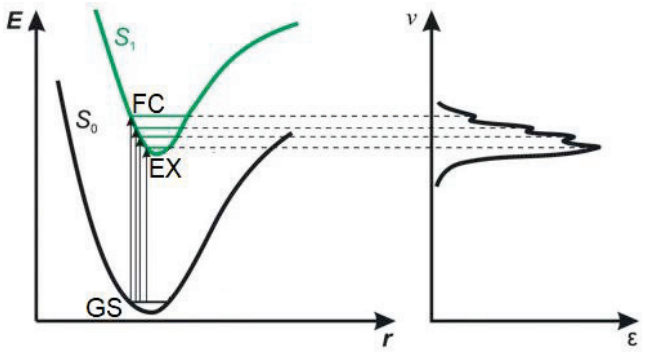

Figure 2. The energetic diagram of vibronic transition

When a photon is absorbed by a molecule of a solute in the ground state (GS), according to the Franck-Condon principle, a redistribution of the electron density occurs in it at constant positions of the nuclei, i.e. the molecule of the solute passes into an excited nonequilibrium (Franck-Condon) state FC (vertical transition). In this case, a similar process (polarization with immobile nuclei) occurs in the nearest solvation shell. After that, the "solute-solvent" system relaxes to the equilibrium excited (EX) state by means of the displacement of the nuclei (Fig. 2).

In our work, we used the methodology of Baiardi et al. for calculating vibrationally resolved electronic spectra of one-photon absorption by the method of TD-DFT, which is described in detail in Ref. [71]. Therefore, here we will only briefly list its main features. The vibronic spectra were calculated using the adiabatic Hessian model, in which the potential energy surfaces (PESs) of the ground and excited states were calculated near their respective equilibrium nuclear coordinates. Both PESs - for ground and excited states (see Fig. 2) - were described in the harmonic approximation. The first-order term corresponds to the Franck-Condon approximation [72], and the second-order term corresponds to the Herzberg-Teller approximation [73]. To calculate the vibronic spectra, we used the general Franck-Condon-Herzberg-Teller method [74]. Ead is the difference between the energies of the ground vibrational states of the ground and excited states, $\chi(t)$ is the vibrational wave function. The temperature T=298 K was taken. In the numerical integration, 2^{18} steps were used and the time interval $\Delta t=2^{18}\times10^{-17}=2.62\times10^{-12}$ s. To broaden the bands of vibronic transitions, we used Gaussians with a full width at half maximum HWHM=600 cm^{-1} (the broadening was chosen so that the calculated spectra corresponded best to the experimental one).

Water is the most difficult medium for implicit accounting due to its specific interactions with solute molecules. Therefore, for a more objective picture, we used PCM (Polarizable Continuum Model with External Integration Formalism - IEF) with its original parameters [75], as well as with atomic radii and non-electrostatic terms of SMD (Solvation Model based on solute electron Density) [76]. IEFPCM calculates the energy in a solution by making the electrostatic potential of the solute self-consistent with the reaction field of the solvent (state-specific approach).

The initial spatial structure of the TBO cation was taken from the ChemSpider database http://www.chemspider.com (ID 11239098). All other calculations were performed using the Gaussian16 software package [77]. The calculation results were visualized using the GaussView software [78].

RESULTS AND DISCUSSION

It is known that the results of TD-DFT calculations of the excited electronic states of organic molecules are largely determined by the functional used [79-82]. Therefore, to calculate the vibronic absorption spectrum of TBO in an aqueous solution, we used all hybrid functionals supported by Gaussian16. Singlet HOMO→LUMO transitions in the visible region of the spectrum were analyzed. We used the 6-31++G(d,p) basis set as well as IEFPCM and SMD solvent models (Fig. 3). The large difference between the values of λ_{vert} and λ_{vibron} stands out. This indicates the importance of considering the vibronic coupling when calculating the absorption spectra. Although direct comparison of λ_{vert} and λ_{exp} is widespread in the literature, it is more correct to compare λ_{vibron} and λ_{exp} [82]. Fig. 3 shows that all functionals with IEFPCM solvent model give an underestimated λvibron values in comparison with the experimental value $\lambda_{max}\approx630$ nm=1.97 eV [9,54,66]. This is a manifestation of the so-called "cyanine failure", which consists in a systematic underestimation of the wavelength by all hybrid functionals with the PCM solvent model. [83-85]. The best result with the IEFPSM solvent model was shown by the O3LYP functional (625 nm=1.98 eV). However, SMD solvent model shows a good agreement with experimental value λmax in combination with X3LYP functional (λ_{vibron}=632 nm=1.96 eV, see Fig. 4). X3LYP [86] is an improved version of very popular B3LYP functional. Therefore, further analysis of vibronic transitions and electronic states of TBO will be carried out at X3LYP/6-31++G(d,p)/SMD theory level.

Note that the solvent model affects the position of the absorption maximum and vibronic transitions; however, on the whole, the band shape remains practically unchanged (see Fig. 4). The calculated vibronic absorption spectrum of TBO (see Fig. 4) in its shape good coincides with the experimental one. It has a pronounced asymmetry (the long-wavelength slope is steeper than the short-wavelength one), but does not have a shoulder, like the spectra of some other thiazine dyes (methylene blue, thionine, azure B, and azure C [87,88]). The thiazine dye Azure A also has a spectrum form similar to TBO [87] and differs from it in the absence of a methyl group in the ortho position. As can be seen from Fig. 4, the asymmetry of the absorption spectrum of the dye is due to vibronic transitions, mainly #7, #8 and #9. The approximation of the spectrum of a diluted dye solution to a symmetric (Gaussian) curve led to a significant shift in the calculated absorption maximum of the monomer (610 nm) with respect to the experimental one (630 nm) [52]. At the same time, such a fit, performed using an arbitrary curve, gave a maximum of the latter at 628 nm [51]. The other (beside HOMO→LUMO) electronic transitions of the TBO molecule in the visible range have low oscillator strength f (Table 1).

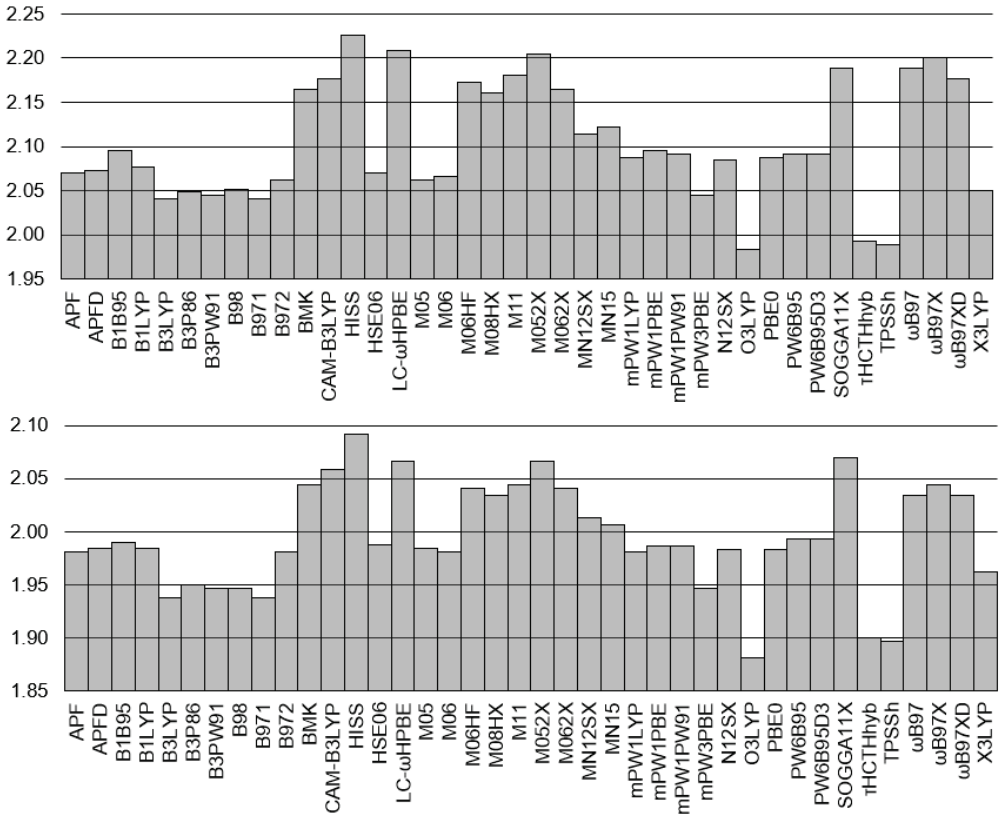

Figure 3. Calculated values of λ_{vibron} (eV) for various functionals with IEFPCM (top) and SMD (bottom) solvent models

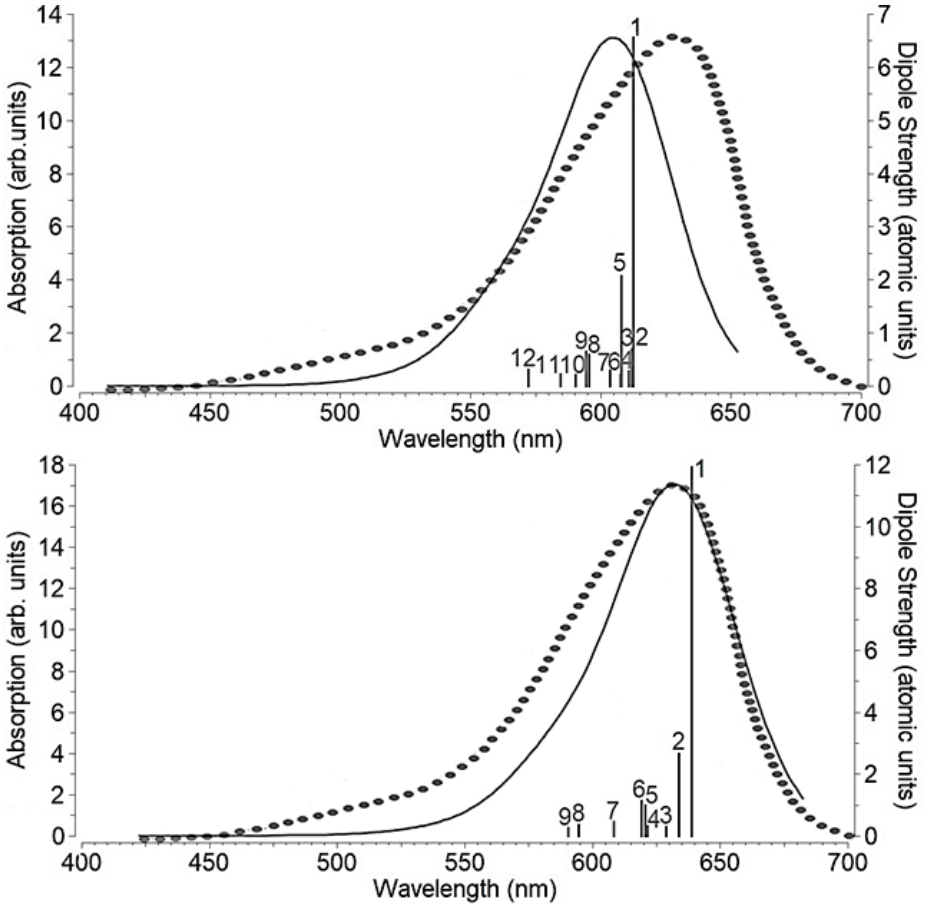

Figure 4. Calculated absorption spectra of TBO molecule (solid lines, X3LYP/6-31++G(d,p)/IEFPCM (top) and X3LYP/6-31++G(d,p)/SMD (bottom) theory levels). Vertical lines are dipole strength of vibronic transitions. Dotted lines: experimental absorption spectrum of TBO (5 μM, 298 K) in aqueous solution from Ref. [51], permission from Elsevier®, order number 5023050596891)

The TBO molecule contains 456 molecular orbitals, of which 71 are occupied and 385 are unoccupied. Thus, MO #71 is the highest occupied (HOMO) and MO #72 is the lowest unoccupied (LUMO). The orbitals involved in the studied electronic transitions are shown in Fig. 5. Their configurations are π- and π*-type, respectively. The differential electron correlation is large (Fig. 5 shows the typical odd/even alternance of cyanines). Comparing HOMO and LUMO, it can be seen that the redistribution of the electron density upon photoexcitation mainly occurs in the central ring of the chromophore.

The most intense vibronic transition (except $0_0 \rightarrow 0^0$) is $0_0 \rightarrow 6^1$ (Table 2, see Fig. 4). The total number of normal vibrational modes of the TBO molecule is 99. The sum of Franck-Condon factors was 99.88%. Thus, the contribution of the Herzberg-Teller effect (see Eq. (2)) turned out to be negligible.

The transition dipole moment M is directed along the x-axis of the chromophore (Table 3) which coincides with the experimental data on the measurement of the dichroism of the dye in a stretched PVA film [70]. A value of M=3.34 a.u. was obtained in Ref. [51] on the basis of spectrophotometric data. The calculated values of the dipole moment μ of the

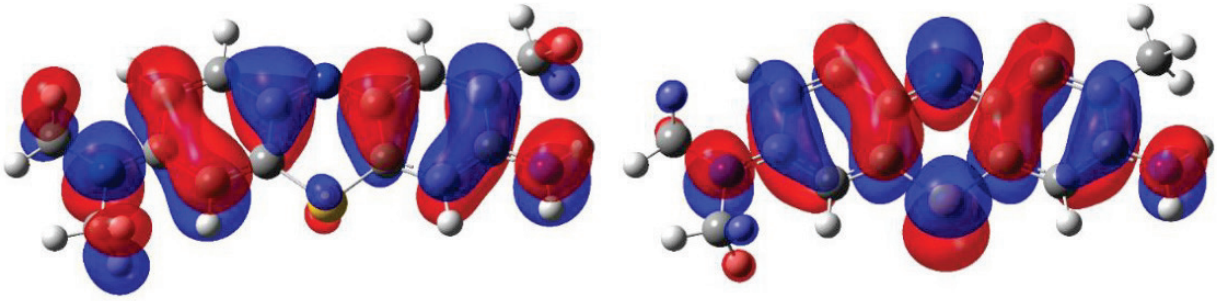

Figure 5. The TBO molecular orbitals between which the investigated electronic transition occurs: HOMO (left) and LUMO (right). Positive lobes are colored red and negative lobes are colored blue

Table 1. The three lowest electronic transitions of TBO

Transition	λ_{vert}		f	Involved transitions
	nm	eV		
$S_0 \rightarrow S_1$	529	2.35	0.8631	HOMO→LUMO
$S_0 \rightarrow S_2$	473	2.62	0.0115	(HOMO-1)→LUMO
$S_0 \rightarrow S_3$	360	3.44	0.0014	(HOMO-4)→LUMO

Table 2. Vibronic absorption transitions in the TBO molecule

#	Transition	λ		$\Delta\nu$ (cm^{-1})	I	p (a.u.)	Vibration description
		nm	eV				
1	$0_0 \rightarrow 0^0$	639	1.94	0	102800	11.9	-
2	$0_0 \rightarrow 6^1$	634	1.96	124	23120	2.66	Flexural vibrations of a chromophore in its plane
3	$0_0 \rightarrow 6^2$	629	1.97	249	2495	0.285	see above
4	$0_0 \rightarrow 23^1$	621	2.00	438	2777	0.314	Compression-stretching of the central ring of the chromophore along the short axis of the latter
	$0_0 \rightarrow 23^1$	621	2.00	463	8754	0.987	Bending vibrations of the side rings of the chromophore in antiphase to each other
6	$0_0 \rightarrow 25^1$	619	2.00	498	10020	1.13	Compression-stretching of the central ring of the chromophore along the long axis of the latter
7	$0_0 \rightarrow 37^1$	608	2.04	784	4196	0.464	
8	$0_0 \rightarrow 54^1$	595	2.08	1168	3316	0.358	Pendulum vibrations of chromophore hydrogen atoms
9	$0_0 \rightarrow 60^1$	590	2.10	1288	2557	0.274	

λ is the wavelength, Δν is the relative frequency, I is the line intensity, and p is the dipole strength

Table 3. Calculated dipole moments (D) and transition electric dipole moments (a.u.) of TBO molecule

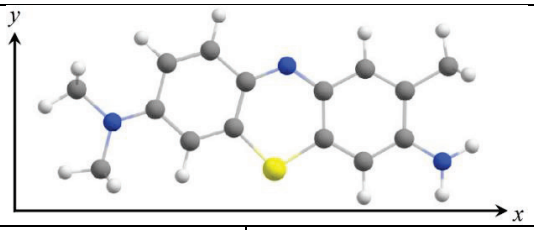

Dipole moment	Ground state	Franck-Condon state	Equilibrium excited state
μx	0.0983	-1.35	-1.83
μy	-3.61	-4.15	-4.42
μz	0.0182	0.0230	0.0301
μ	3.61	4.37	4.78
Ground to Franck-Condon state transition electric dipole moments			
Mx	-5.11		
My	0.504		
Mz	-0.0007		
M^2	26.4		

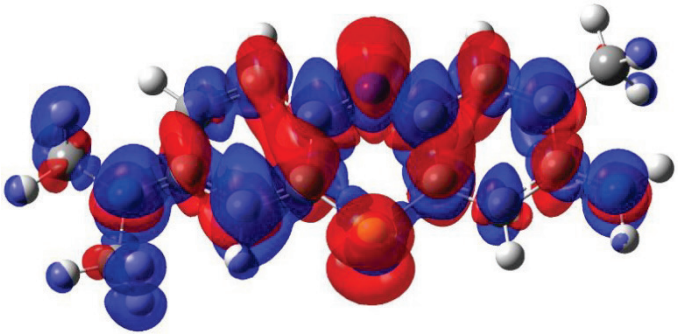

Figure 6. The electron density difference between Franck-Condon and ground states of TBO molecule. Areas of positive values are colored red and areas of negative values are colored blue

TBO molecule in the excited state turn out to be larger than in the ground state: $\mu_{EX}>\mu_{FC}>\mu_{GS}$. This indicates the predominance of the $\pi\rightarrow\pi^*$ transition type [89]. This also means a stronger interaction with the solvent of the TBO molecule in the excited state compared to the ground state, and is consistent with its slight positive solvatochromism (in methanol λ_{max}=629 nm [7], and in water λ_{max}=630 nm [9,54,66]). Note that the authors of Ref. [48] also assert the $\pi\rightarrow\pi^*$ type of TBO electronic transition.

CONCLUSIONS

In this work, we calculated the vibronic absorption spectrum of the thiazine dye Toluidine blue O in an aqueous solution using TD-DFT, all hybrid functionals supported by Gaussian16 software, 6-31++G(d,p) basis set, and two solvent models (IEFPCM and SMD). The IEFPCM solvent model showed overestimated transition energies for all used functionals, demonstrating the well- known "cyanine failure". At the same time, the SMD model in combination with the X3LYP functional gave excellent agreement with the experiment. The electronic properties of the ground and excited states of the dye were also investigated: the dipole moments and atomic charges were calculated; the distribution maps of the electron density were built. Photoexcitation leads to an increase in the dipole moment of the dye molecule. In accordance with our results, the absorption peak of the Toluidine blue O solution in the visible region of the spectrum is due to the electronic transition of $\pi\rightarrow\pi^*$ type.

References:

1. Fekrazad R., Zare H., Mohammadi S., Vand S. Photodynamic therapy effect on cell growth inhibition induced by Radachlorin and toluidine blue O on Staphylococcus aureus and Escherichia coli: An in vitro study, Photodiagn. *Photodyn. Ther*., 2016, vol. 15, pp. 213-217, doi: 10.1016/j.pdpdt.2016.07.001.

2. Anju V.T., Paramanantham P., Lal S.B.S., Sharan A., Syed A., Bahkali N.A., Alsaedi M.H., Kaviyarasu K., Busi S. Antimicrobial photodynamic activity of toluidine blue-carbon nanotube conjugate against Pseudomonas aeruginosa and Staphylococcus aureus - Understanding the mechanism of action. *Photodiagn. Photodyn. Ther*., 2019, vol. 27, pp. 305-316, doi: 10.1016/j.pdpdt.2019.06.014.

3. Moslemi N., Rouzmeh N., Shakerinia F., Bahador A., Azar P.S., Kharazifard M.J., Paknejad M., Fekrazad R. Photodynamic Inactivation of Porphyromonas gingivalis utilizing Radachlorin and Toluidine Blue O as Photosensitizers: An In Vitro Study. *J. Lasers Med. Sci*., 2018, vol. 9, pp. 107-112, doi: 10.15171/jlms.2018.21.

4. Parasuraman P., Antony A.P., Lal S.B.S., Sharan A., Siddhardha B., Kasinathan K., Bahkali N.A., Dawoud T.M.S., Syed A. Antimicrobial photodynamic activity of toluidine blue encapsulated in mesoporous silica nanoparticles against Pseudomonas aeruginosa and Staphylococcus aureus. *Biofouling*, 2019, vol. 35, pp. 89-103, doi: 10.1080/08927014.2019.1570501.

5. Almeida A.M., Oliveira O.N., Aoki P.H.B. Role of Toluidine Blue‐O Binding Mechanism for Photooxidation in Bioinspired Bacterial Membranes. *Langmuir*, 2019, vol. 35, pp. 16745-16751, doi: 10.1021/acs.langmuir.9b03045.

6. Misba L., Kulshrestha S., Khan A.U. Antibiofilm action of a toluidine blue O-silver nanoparticle conjugate on Streptococcus mutans: a mechanism of type I photodynamic therapy. *Biofouling*, 2016, vol. 32, pp. 313-328, doi: 10.1080/08927014.2016.1141899.

7. Wainwright M., O'Kane C., Rawthore S. Phenothiazinium photosensitisers XI. Improved toluidine blue photoantimicrobials. *J. Photochem. Photobiol. B*, 2016, vol. 160, pp. 68-71, doi: 10.1016/j.jphotobiol.2016.03.035.

8. Rolim J.P.M.L., de-Melo M.A.S., Guedes S.F., Albuquerque-Filho F.B., de Souza J.R., Nogueira N.A.P., Zanin I.C.J., Rodrigues L.K.A. The antimicrobial activity of photodynamic therapy against Streptococcus mutans using different photosensitizers. *J. Photochem. Photobiol. B*, 2012, vol. 106, pp. 40-46, doi: 10.1016/j.jphotobiol.2011.10.001.

9. Drzymala R.E., Liebman P.A., Romhanyi G. Acid Polysaccharide Content of Frog Rod Outer Segments Determined by metachromatic Toluidine Blue Staining. *Histochemistry*, 1982, vol. 76, pp. 363-379, doi: 10.1007/BF00543958.

10. Bastos A.L., Marques D.V., da Silva J.F., Nunes J.B.M., Correia A.D., Vigariox J.D., Terrinha A.M. Primary Inducible Fluorescence in Secretory Granules of Tumor Cells Supravitally Stained by a Toluidine Blue Dye. *Z. Naturforschg*, 1968, vol. 23b, pp. 969-975, doi: 10.1515/znb-1968-0716.

11. Sridharan G., Shankar A.A. Toluidine blue: A review of its chemistry and clinical utility. *J. Oral Maxillofac. Pathol*., 2012, vol. 16, pp. 251-255, doi: 10.4103/0973-029X.99081.

12. Li X., Yuan R., Chai Y., Zhang L., Zhuo Y., Zhang Y. Amperometric immunosensor based on toluidine blue/nano-Au through electrostatic interaction for determination of carcinoembryonic antigen. *J. Biotechnol*., 2006, vol. 123, pp. 356-366, doi: 10.1016/j.jbiotec.2005.11.023.

13. Bai X., Chen G., Shiu K.-K. Electrochemical biosensor based on reduced graphene oxide modified electrode with Prussian blue and poly(toluidine blue O) coating. *Electrochim. Acta*, 2013, vol. 89, pp. 454-460, doi: 10.1016/j.electacta.2012.11.086.

14. Gao H.-W., Qin P., Lin C., Shang Z.-M., Sun W. Electrochemical DNA Biosensor for the Detection of Listeria Monocytogenes Using Toluidine Blue as a Hybridization Indicator. *J. Iran. Chem. Soc*., 2010, vol. 7, pp. 119-127, doi: 10.1007/BF03245868.

15. Liu M., Zhang G.Shi.L., Zhao G., Jin L. Electrode modified with toluidine blue-doped silica nanoparticles, and its use for enhanced amperometric sensing of hemoglobin. *Anal. Bioanal. Chem*., 2008, vol. 391, pp. 1951-1959, doi: 10.1007/s00216-008-2103-z.

16. Gligor D., Walcarius A. Glassy carbon electrode modified with a film of poly(Toluidine Blue O) and carbon nanotubes for nitrite detection. *J. Solid State Electrochem*., 2014, vol. 18, pp. 1519-1528, doi: 10.1007/s10008-013-2365-z.

17. Zeyada H.M., Youssif M.I., El‐Ghamaz N.A., Nasher M.A. Carrier transport mechanisms and photovoltaic characteristics of Au/toluidine blue/n-Si/Al heterojunction solar cell. *J. Mater. Sci.: Mater. Electronics*, 2018, vol. 29, pp. 3592-3601, doi: 10.1007/s10854-017-8289-0.

18. Viswanath V., Nair S.S., Subodh G., Muneera C.I. Emission features, surface morphology and optical limiting properties of semiconducting Toluidine Blue O dye‐poly(vinyl alcohol) nanocomposite architecture. *SN Appl. Sci*., 2019, vol. 1, no. 43, doi: 10.1007/s42452-018-0043-6.

19. Dubey T., Gorantla N.V., Chandrashekara K.T., Chinnathambi S. Photoexcited Toluidine Blue Inhibits Tau Aggregation in Alzheimer's Disease. *ACS Omega*, 2019, vol. 4, pp. 18793-18802. doi: 10.1021/acsomega.9b02792.

20. Ilanchelian M., Ramaraj R. Binding Interactions of Toluidine Blue O with Escherichia Coli DNA: Formation of Bridged Structure. *J. Fluoresc*., 2011, vol. 21, pp. 1439-1453, doi: 10.1007/s10895- 010-0829-4.

21. Sato S., Matsumoto S., Freivalds T., Erenpreisa J. Consideration on the Metachromatic Spectra of Toluidine Blue Dimers Formed on DNA Oligomers. *Bull. Chem. Soc. Jpn*., 2010, vol. 83, pp. 1216-1222, doi: 10.1246/bcsj.20100032.

22. Chi Z., Liu R., Sun Y., Wang M., Zhang P., Gao C. Investigation on the toxic interaction of toluidine blue with calf thymus DNA. *J. Hazard. Mater*., 2010, vol. 175, pp. 274-278, doi: 10.1016/j.jhazmat.2009.09.160.

23. Wang J., Yang X. Multiplex binding modes of toluidine blue with calf thymus DNA and conformational transition of DNA revealed by spectroscopic studies. *Spectrochim. Acta A*, 2009, vol. 74, pp. 421-426, doi: 10.1016/j.saa.2009.06.038.

24. Paul P., Kumar G.S. Thermodynamics of the DNA binding of phenothiazinium dyes toluidine blue O, azure A and azure B. *J. Chem. Thermodynamics*, 2013, vol. 64, pp. 50-57, doi: 10.1016/j.jct.2013.04.023.

25. Chen L.-H., Nie Y.-T., Liu L.-Z., Shen H.-X. Determination of Nucleic Acids on the Basis of Enhancement Effect of Resonance Light Scattering of Toluidine Blue. *Anal. Lett*., 2003, vol. 36, pp. 107-122, doi: 10.1081/AL-120017266.

26. Paul P., Mati S.S., Bhattacharya S.C., Kumar G.S. Spectroscopic, calorimetric, cyclic voltammetric and molecular modeling studies of new methylene blue-polyadenylic acid interaction and comparison to thionine and toluidine

blue O: Understanding self-structure formation by planar dyes. *Dyes Pigments*, 2017, vol. 136, pp. 205-218, doi: 10.1016/j.dyepig.2016.08.027.

27. Paul P., Kumar G.S. Targeting ribonucleic acids by toxic small molecules: Structural perturbation and energetics of interaction of phenothiazinium dyes thionine and toluidine blue O to $tRNA^{phe}$. *J. Hazard. Mater*., 2013, vol. 263, pp. 735-745, doi: 10.1016/j.jhazmat.2013.10.040.

28. Liu J., Zou A., Mu B. Toluidine blue: Aggregation properties and distribution behavior in surfactin micelle solution. *Colloids Surfaces B*, 2010, vol. 75, pp. 496-500, doi: 10.1016/j.colsurfb.2009.09.025.

29. Shanmugaraj K., Umadevi P., Senthilkumar L., Ilanchelian M. Elucidation of binding mechanism of photodynamic therapeutic agent toluidine blue O with chicken egg white lysozyme by spectroscopic and molecular dynamics studies. *Photochem. Photobiol*., 2017, vol. 93, pp. 1043-1056, doi: 10.1111/php.12744.

30. Sharma A.S., Anandakumar S., Ilanchelian M. A combined spectroscopic and molecular docking study on site selective binding interaction of Toluidine blue O with Human and Bovine serum albumins. *J. Luminesc*., 2014, vol. 151, pp. 206-218, doi: 10.1016/j.jlumin.2014.02.009.

31. Saha B., Chowdhury S., Sanyal D., Chattopadhyay K., Kumar G.S. Comparative Study of Toluidine Blue O and Methylene Blue Binding to Lysozyme and Their Inhibitory Effects on Protein Aggregation. *ACS Omega*, 2018, vol. 3, pp. 2588-2601, doi: 10.1021/acsomega.7b01991.

32. Ganguly B., Nath R.K., Panda A.K. Spectral Studies on the Interaction of Toluidine Blue O with Bovine Serum Albumin. *J. Surface Sci. Technol*., 2013, vol. 29, pp. 1-16.

33. Shanmugaraj K., Anandakumar S., Ilanchelian M. Unraveling the binding interaction of Toluidine blue O with bovine hemoglobin - a multi spectroscopic and molecular modeling approach. *RSC Adv*., 2015, vol. 5, pp. 3930-3940, doi: 10.1039/c4ra11136b.

34. Wang J., Guo Y., Liu B., Cheng C., Wang Z., Han G., Gao J., Zhang X. Spectroscopic analyses on interaction of bovine serum albumin (BSA) with toluidine blue (TB) and its sonodynamic damage under ultrasonic irradiation. *J. Luminesc*., 2011, vol. 131, pp. 231-237, doi: 10.1016/j.jlumin.2010.10.003.

35. Yu M.- E., Cheong B.- S., Cho H.- G. SERS Spectroscopy and DFT Studies of Thionine and its Derivatives Adsorbed on Silver Colloids: Which N Atom is Used for Coordination of a Phenothiazine- Based Natural Dye to Electron-Deficient Metal Surface? *Bull. Korean Chem. Soc*., 2017, vol. 38, pp. 928-934, doi: 10.1002/bkcs.11205.

36. Aranaz I., Alcantara A.R., Heras A., Acosta N. Efficient reduction of Toluidine Blue O dye using silver nanoparticles synthesized by low molecular weight chitosans. *Int. J. Biol. Macromol*., 2019, vol. 131, pp. 682-690, doi: 10.1016/j.ijbiomac.2019.03.119.

37. Neelakandeswari N., Sangami G., Dharmaraj N., Taek N.K., Kim H.Y. Spectroscopic investigations on the photodegradation of toluidine blue dye using cadmium sulphide nanoparticles prepared by a novel method. *Spectrochim. Acta A*, 2011, vol. 78, pp. 1592-1598, doi: 10.1016/j.saa.2011.02.008.

38. Xie X., Guo H., Yan M., Korshin G. Interactions between natural organic matter (NOM) and the cationic dye toluidine blue at varying pHs and ionic strengths: Effects of NOM charges and Donnan gel potentials. *Chemosphere*, 2019, vol. 236, p. 124272, doi: 10.1016/j.chemosphere.2019.07.003.

39. Ilanchelian M., Raj C.R., Ramaraj R. Spectral Studies on the Cyclodextrin Inclusion Complexes of Toluidine Blue O and Meldola's Blue in Aqueous Solution. *J. Incl. Phenom. Macrocycl. Chem.*, 2000, vol. 36, pp. 9-20, doi: 10.1023/A:1008085829227.

40. Dasmandal S., Bhattacharyya D., Rudra S., Patel B.K., Mahapatra A. Spectroscopic investigation on interaction of toluidine blue/AOT/γ-cyclodextrin ternary system. *J. Luminesc*., 2016, vol. 179, pp. 340-349, doi: 10.1016/j.jlumin.2016.06.057.

41. Yuan Z., Zhu M., Han S. Supramolecular inclusion complex formation and application of β-cyclodextrin with heteroanthracene ring cationic dyes. *Anal. Chim. Acta*, 1999, vol. 389, pp. 291-298, doi: 10.1016/S0003-2670(99)00134-8.

42. Arikan B., Tuncay M. The effect of SDS micelles on reduction of toluidine blue by ascorbic acid inm acid medium. *Colloids Surf. A*, 2006, vol. 273, pp. 202-207, doi: 10.1016/j.colsurfa.2005.08.025.

43. Mohamed A.A., Ulber R., Zayed A. Chitosan-Toluidine Blue Beads for Purification of Fucoidans. *Carbohydrate Polymers*, 2020, vol. 231, p. 115686, doi: 10.1016/j.carbpol.2019.115686.

44. D'Ilario I.L., Francolini I., Martinelli A., Piozzi A. Insight into the Heparin-Toluidine Blue (C.I. Basic Blue 17) interaction. *Dyes Pigments*, 2009, vol. 80, pp. 343-348, doi: 10.1016/j.dyepig.2008.07.015.

45. Robinson-Duggon J., Pizarro N., Gunther G., Ziniga- Nunez D., Edwards A.M., Greer A., Fuentealba D. Fatty Acid Conjugates of Toluidine Blue O as Amphiphilic Photosensitizers: Synthesis, Solubility, Photophysics and Photochemical Properties. *Photochem. Photobiol*., 2021, vol. 97, pp. 71-79, doi: 10.1111/php.13304.

46. Kiraly K., Lapvetelainen T., Arokoski J., Torronen K., Modis L., Kiviranta I., Helminen H.J. Application of selected cationic dyes for the semiquantitative estimation of glycosaminoglycans in histological sections of articular cartilage by microspectrophotometry. *Histochem. J*., 1996, vol. 28, pp. 577-590, doi: 10.1007/BF02331378.

47. Hahn T., Schulz M., Stadtmuller R., Zayed A., Muffler K., Lang S., Ulber R. Cationic dye for the specific determination of sulfated polysaccharides. *Anal. Lett*., 2016, vol. 49, pp. 1948-1962, doi: 10.1080/00032719.2015.1126839.

48. Hahn T., Muffler K., Ulber R. Isothermal microcalorimetric studies of toluidine blue O/sulfated polysaccharides interactions. *J. Therm. Anal. Calorim*., 2016, vol. 123, pp. 2291-2296, doi: 10.1007/s10973-015-5101-3.

49. Fradj A.B., Lafi R., Gzara L., Hamzaoui A.H., Hafiane A. Spectrophotometric study of the interaction of toluidine blue with poly(ammonium acrylate). *J. Mol. Liquids*, 2014, vol. 194, pp. 110-114, doi: 10.1016/j.molliq.2014.01.008.

50. Ushio H., Yasunaga T., Sano T., Tsuji Y. Kinetic Study of Cooperative Binding Reaction of Toluidine Blue to Poly (α,L-glutamic acid) by Means of the Electric-Field Pulse Method. *Biopolymers*, 1976, vol. 15, pp. 187-201, doi: 10.1002/bip.1976.360150113.

51. Ghanadzadeh Gilani A., Poormohammadi-Ahandani Z., Kian R. Additive-induced aggregate changes of two structurally similar dyes in aqueous solutions: A comparative photophysical study. *Spectrochim. Acta*, 2018, vol. 189, pp. 543-555, doi: 10.1016/j.saa.2017.08.048.

52. D'Ilario L., Martinelli A. Toluidine blue: aggregation properties and structural aspects. *Modelling Simul. Mater. Sci. Eng*., 2006, vol. 14, pp. 581-595, doi: 10.1088/0965-0393/14/4/003.

53. Matassa R., Sadun C., D'Ilario L., Martinelli A., Caminiti R. Supramolecular Organization of Toluidine Blue Dye in Solid Amorphous Phases. *J. Phys. Chem. B*, 2007, vol. 111, pp. 1994-1999, doi: 10.1021/jp066555j.

54. Usacheva M.N., Teichert M.C., Biel M.A. The role of the methylene blue and toluidine blue monomers and dimers in the photoinactivation of bacteria. *J. Photochem. Photobiol. B*, 2003, vol. 71, pp. 87-98, doi: 10.1016/j.jphotobiol.2003.06.002.

55. Jonnalagadda S.B., Tshabalala D. A Kinetic Study of the Reduction of Toluidine Blue with Thiourea in Acidic Solution. *Int. J. Chem. Kinetics*, 1992, vol. 24, pp. 999-1007, doi: 10.1002/kin.550241110.

56. Arikan B., Tuncay M. Micellar effects and reactant incorporation in reduction of toluidine blue by ascorbic acid. Dyes Pigments, 2005, vol. 64, pp. 1-8, doi: 10.1016/j.dyepig.2004.03.013.

57. Mahadevan J., Guha S.N., Kishore K., Moorthy P.N. One-electron reduction of toluidine blue. A pulse radiolysis study. *Proc. Indian Acad. Sci. (Chem. Sci.)*, 1989, vol. 101, pp. 43-53, doi: 10.1007/BF02869385.

58. Mosleh S., Rahimi M.R., Ghaedi M., Dashtian K., Hajati S. BiPO4/Bi2S3-HKUST-1-MOF as novel blue light-driven photocatalyst for simultaneous degradation of toluidine blue and auramine-O dyes in new rotating packed bed reactor: optimization and comparison to conventional reactor. *RSC Adv*., 2016, vol. 6, pp. 63667-63680, doi: 10.1039/C6RA10385E.

59. Singh H.K., Saquib M., Haque M.M., Muneer M. Heterogeneous photocatalysed decolorization of two selected dye derivatives neutral red and toluidine blue in aqueous suspensions. *Chem. Eng. J*., 2008, vol. 136, pp. 77-81, doi: 10.1016/j.cej.2007.05.009.

60. Robinson-Duggon J., Marino-Ocampo N., Barrias P., Zuniga-Nuunez D., Gunther G., Edwards A.M., Greer A., Fuentealba D. Mechanism of Visible-Light Photooxidative Demethylation of Toluidine Blue O. *J. Phys. Chem. A*, 2019, vol. 123, pp. 4863-4872, doi: 10.1021/acs.jpca.9b03588.

61. Mandal N.C., Biswas B.B. Metachromasia Induced by Inositol-Hexa-Phosphate with Toluidine Blue. *Histochemie*, 1969, vol. 18, pp. 202-209, doi: 10.1007/BF00306167.

62. Vleugels L.F.W., Ricois S., Voets I.K., Tuinier R. Reversal of metachromasy revisited; displacement of Toluidine-blue from alginate by surfactants. *Colloids Surf. A*, 2017, vol. 529, pp. 454-461, doi: 10.1016/j.colsurfa.2017.06.027.

63. Azariah J. Studies on metachromasia. 1. The non-specificity of green metachromasia to toluidine blue. *Acta Histochem*., 1972, vol. 43, pp. 254-259.

64. Mazeikiene R., Niaura G., Eicher-Lorka O., Malinauskas A. Raman spectroelectrochemical study of Toluidine Blue, adsorbed and electropolymerized at a gold electrode. *Vibr. Spectrosc*., 2008, vol. 47, pp. 105-112, doi: 10.1016/j.vibspec.2008.02.018.

65. McKamey M.R., Spitznagle L.A. Chromatographic, Mass Spectral, and Visible Light Absorption Characteristics of Toluidine Blue O and Related Dyes. *J. Pharm. Sci*., 1975, vol. 64, pp. 1456-1452, doi: 10.1002/jps.2600640907.

66. Woislawski S. The Spectrophotometric Determination of Ionization Constants of Basic Dyes. *J. Am. Chem. Soc*., 1953, vol. 75, pp. 5201-5203, doi: 10.1021/ja01117a016.

67. Nasher M.A., Youssif M.I., El-Ghamaz N.A., Zeyada H.M. Linear and Nonlinear Optical Properties of Irradiated Toluidine Blue Thin Films. *Optik*, 2019, vol. 178, pp. 532-543, doi: 10.1016/j.ijleo.2018.10.001.

68. Nasher M.A., Youssif M.I., El-Ghamaz N.A., Zeyada H.M. Structural, optical and electrical studies of Toluidine Blue thin films prepared by thermal evaporation technique. *J. Luminesc*., 2018, vol. 204, pp. 428-435, doi: 10.1016/j.jlumin.2018.08.037.

69. Viswanath V., Muneera C.I. Nonlinear Refraction Behaviour of Toluidine Blue O Dye-PVA Nanocomposite Films under CW Laser Light Excitation. *Mater. Today Proc*., 2017, vol. 4, pp. 4412-4416, doi: 10.1016/j.matpr.2017.04.013.

70. Platonova N.V., Popov K.R. Electronic states in the acridine and phenothiazine dye molecules. *J. Appl. Spectrosc*., 1979, vol. 30, pp. 321-326, doi: 10.1007/BF00608271.

71. Baiardi A., Bloino J., Barone V. General Time Dependent Approach to Vibronic Spectroscopy Including Franck-Condon, Herzberg-Teller, and Duschinsky Effects. *J. Chem. Theory Comput*., 2013, vol. 9, pp. 4097-115, doi: 10.1021/ct400450k.

72. Condon E.U. Nuclear motions associated with electron transitions in diatomic molecules. *Phys. Rev*., 1928, vol. 32, pp. 858-872, doi: 10.1103/PhysRev.32.858.

73. Herzberg G., Teller E. Schwingungsstruktur der Elektronenubergange bei mehratomigen Molekulen. *Z. Phys. Chem., Abt. B*, 1933, vol. 21, pp. 410-446, doi: 10.1515/zpch-1933-2136.

74. Santoro F., Lami A., Improta R., Bloino J., Barone V. Effective method for the computation of optical spectra of large molecules at finite temperature including the Duschinsky and Herzberg-Teller effect: The Q_X band of porphyrin as a case study. *J. Chem. Phys*., 2008, vol. 128, p. 224311, doi: 10.1063/1.2929846.

75. Improta R., Barone V., Scalmani G., Frisch M.J. A state-specific polarizable continuum model time dependent density functional method for excited state calculations in solution. *J. Chem. Phys*., 2006, vol. 125, p. 054103, doi: 10.1063/1.2222364.

76. Marenich A.V., Cramer C.J., Truhlar D.G. Universal solvation model based on solute electron density and a continuum model of the solvent defined by the bulk dielectric constant and atomic surface tensions. *J. Phys. Chem. B*, 2009, vol. 113, pp. 6378-6396, doi: 10.1021/jp810292n.

77. Frisch M.J., Trucks G.W., Schlegel H.B., et al. *Gaussian 16*, Revision C.01, Inc., Wallingford CT, 2016.

78. Dennington R., Keith T.A., Millam J.M. *GaussView*, Version 6.1, Semichem Inc., Shawnee Mission KS, 2016.

79. Dierksen M., Grimme S. The Vibronic Structure of Electronic Absorption Spectra of Large Molecules: A Time-Dependent Density Functional Study on the Influence of "Exact" Hartree-Fock Exchange. *J Phys Chem A*, 2004, vol. 108, pp. 10225-10237, doi: 10.1021/jp047289h.

80. Jacquemin D., Bremond E., Planchat A., Ciofini I., Adamo C. TD-DFT vibronic couplings in anthraquinones: from basis set and functional benchmarks to applications for industrial dyes. *J. Chem. Theory Comput*., 2011, vol. 7, pp. 1882-1892, doi: 10.1021/ct200259k.

81. Adamo C., Jacquemin D. The calculations of excited-state properties with Time-Dependent Density Functional Theory. *Chem. Soc. Rev*., 2013, vol. 42, pp. 845-856, doi: 10.1039/C2CS35394F.

82. Jacquemin D., Bremond E., Ciofini I., Adamo C. Impact of Vibronic Couplings on Perceived Colors: Two Anthraquinones as a Working Example. *J. Phys. Chem. Lett*., 2012, vol. 3, pp. 468-471, doi: 10.1021/jz201552x.

83. Jacquemin D., Zhao Y., Valero R., Adamo C., Ciofini I., Truhlar D.G. Verdict: Time-Dependent Density Functional Theory "Not Guilty" of Large Errors for Cyanines. *J. Chem. Theory Comput*., 2012, vol. 8, pp. 1255-1259, doi: 10.1021/ct200721d.

84. Le Guennic B., Jacquemin D. Taking Up the Cyanine Challenge with Quantum Tools. *Acc. Chem. Res*., 2015, vol. 48, pp. 530-537, doi: 10.1021/ar500447q.

85. Zhou P. Why the lowest electronic excitations of rhodamines are overestimated by time-dependent density functional theory. *Int. J. Quantum Chem*, 2018, vol. 118, e25780, doi: 10.1002/qua.25780.

86. Xu X., Goddard W.A. The X3LYP extended density functional for accurate descriptions of nonbond interactions, spin states, and thermochemical properties. *Proc. Natl Acad. Sci. USA*, 2004, vol. 101, pp. 2673-2677, doi: 10.1073/pnas.0308730100.

87. Paul P., Mati S.S., Bhattacharya S.C., Kumar G.S. Exploring the interaction of phenothiazinium dyes methylene blue, new methylene blue, azure A and azure B with $tRNA^{Phe}$: spectroscopic, thermodynamic, voltammetric and molecular modeling approach. *Phys. Chem. Chem. Phys*., 2017, vol. 19, pp. 6636-6653, doi: 10.1039/C6CP07888E.

88. Ghanadzadeh Gilani A., Ghorbanpour T., Salmanpour M. Additive effect on the dimer formation of thiazine dyes. *J. Mol. Liquids*, 2013, vol. 177, pp. 273-282, doi: 10.1016/j.molliq.2012.09.005.

89. Reichardt C. Solvatochromic Dyes as Solvent Polarity Indicators. *Chem. Rev*., 1994, vol. 94, pp. 2319-2358, doi: 10.1021/cr00032a005.